Viscous conducting flows with smooth-particle applied mechanics

Oyeon Kum and William G. Hoover
Department of Applied Science, University of California at Davis/Livermore and Lawrence Livermore National Laboratory, Livermore, California 94551-7808

Harald A. Posch
Institute for Experimental Physics, University of Vienna, Boltzmanngasse 5, Vienna A-1090, Austria
(Received 26 May 1995)

Smooth-particle methods have a 20-year history of solving complex problems in fluid and solid mechanics. Here we first discuss the method, pointing out an interesting and fruitful parallel linking smooth-particle methods to atomistic molecular dynamics. We then assess the accuracy and applicability of the method by comparing a set of smooth-particle Rayleigh-Bénard problems, all in the laminar regime, to corresponding highly accurate grid-based numerical solutions of the continuum equations. Both transient and stationary smooth-particle solutions reproduce the grid-based data with velocity errors on the order of a few percent.

PACS number(s): 66.20.+d, 03.40.Gc, 05.70.Ln

I. INTRODUCTION

Smooth-particle applied mechanics [1–6] is a grid-free particle method for solving the *partial* differential equations of fluid or solid mechanics. It is equally applicable in one, two, and three space dimensions. The mass, momentum, and energy of a simulated flow are all calculated by summing up particle contributions. Each particle is smoothly distributed in space according to a "weight function" or "smoothing function" $w(r)$. The smooth-particle formulation simplifies the calculation of the corresponding spatial derivatives $\{\nabla\rho, \nabla\mathbf{v}, \nabla T(\rho,e)\}$ and the comoving fluxes $\{\mathbf{P},\mathbf{Q}\}$ in such a way as to provide the right-hand sides of *ordinary* differential equations for the time development of the particle positions, velocities, and energies $\{\dot{\mathbf{r}}, \dot{\mathbf{v}} \equiv \ddot{\mathbf{r}}, \dot{e}\}$. Thus the mathematical structure of this macroscopic continuum solution method resembles that of the ordinary differential equations of microscopic atomistic molecular dynamics. We discuss the weight function, which characterizes the method, as well as the formulation and structure of the associated ordinary differential equations, in Sec. II. We emphasize and discuss the connection with molecular dynamics in Sec. III.

Like molecular dynamics, smooth-particle methods can be applied in two or three space dimensions nearly as easily as in one. Their implementation on parallel computers is also straightforward. For these two reasons, smooth-particle methods are often applied to complex astrophysical problems [1,2] such as colliding planets and stars, for which correct answers are unknown and grid-based methods are prohibitively expensive. To evaluate the adaptability and fitness of this method to more typical problems in applied mechanics [3], we have recently carried out a detailed investigation [4,5]. Here we describe the application of this technique to a fundamental hydrodynamic instability problem, the Rayleigh-Bénard problem of convective heat conduction in a gravitating fluid heated from below [7–11].

For simplicity, but without lack of generality, we study the Rayleigh-Bénard problem in two dimensions. The required details appear in Sec. IV. These include the equilibrium and nonequilibrium constitutive relations, as well as the thermomechanical boundary conditions required to contain and drive convecting systems. In Sec. V we generate and summarize conventional grid-based continuum results with which our smooth-particle simulations can be compared. We find that the smooth-particle velocities agree with the accurate grid-based data within a few percent.

The continuum results we obtain in Sec. V show an interesting very nearly linear dependence of the flow's kinetic energy per particle K/N on the inverse square root of the Rayleigh number, $\mathrm{Ra}^{-1/2}$ [$\mathrm{Ra} \equiv g\alpha L^3 \Delta T/(\nu\kappa)$], for a factor-of-2 change in $\mathrm{Ra}^{-1/2}$. This simple relationship facilitates the comparison of our smooth-particle results, discussed in Sec. VI, with fully converged continuum predictions. Section VII is devoted to the conclusions we draw from our study.

II. BASIC EQUATIONS OF SMOOTH-PARTICLE APPLIED MECHANICS

Lucy and Monaghan have independently developed the smooth-particle approach [1,2] to solving the usual evolution equations—the continuity equation, the equation of motion, and the energy equation—for a continuum fluid or solid:

$$d\ln\rho/dt = -\nabla\cdot\mathbf{v} ,$$

$$d\mathbf{v}/dt \equiv -(1/\rho)\nabla\cdot\mathbf{P} ,$$

$$de/dt \equiv -(1/\rho)[\nabla\mathbf{v}:\mathbf{P} + \nabla\cdot\mathbf{Q}] .$$

The notation for the flow variables is standard, and it is written here in terms of the time derivatives *following the flow,* the "comoving" or "Lagrangian" derivatives.

Each individual smooth particle is distributed in space according to its smooth weight function $w(r<h)$. As a result, the flow variables and their spatial gradients all take the form of sums involving all particle pairs that lie within the range h of the weight function. The density is a simple summed superposition of smooth-particle contributions. At the location $\mathbf{r}$, the density $\rho(\mathbf{r})$ can be calculated by summing up contributions of all particles at locations $\{\mathbf{r}_j\}$ lying within a cutoff distance h of the location $\mathbf{r}$:

$$\rho(\mathbf{r}) \equiv \sum_j m_j w(\mathbf{r}-\mathbf{r}_j) \ .$$

In its motion, the jth smooth particle carries with it a mass m_j, moves at a velocity v_j, and carries with it a total energy made up of internal and kinetic parts: $m_j[e_j+(v_j^2/2)]$.

For simplicity, in the present work we choose all of the smooth-particle masses equal to a constant mass m. The time development of the individual particle velocities and energies is described below by ordinary differential motion and energy equations. To find the local flow density requires only a simple sum rather than the integration of the conventional continuity equation.

In the smooth-particle work described here we use either Lucy's form [1] or Monaghan's "B-spline" form [2] of the weight function w:

$$w_{\text{Lucy}}(0<r<3\sigma)=(5/9\pi\sigma^2)[1+(r/\sigma)][1-(r/3\sigma)]^3 \ ,$$

$$w_{\text{Monaghan}}(0<r<1.5\sigma)$$
$$=(40/63\pi\sigma^2)[1-(2/3)(r/\sigma)^2+(2/9)(r/\sigma)^3] \ .$$

$$w_{\text{Monaghan}}(1.5\sigma<r<3\sigma)=(80/63\pi\sigma^2)[1-(r/3\sigma)]^3 \ .$$

See Fig. 1. We have arbitrarily chosen the range of the weight functions, h, the "cutoff" distance, equal to 3σ, to be about three times the nearest-neighbor distance for all particles. Despite this finite range, and despite the spline nature of Monaghan's weighting function, both choices have been judiciously constructed to have continuous first and second derivatives for *all* r. The two vanishing derivatives at the cutoff enhance the smoothness of the field variables as well as the ease of integrating the motion and energy equations.

The spatial integral of any smooth-particle weight function is, by definition, unity. In two dimensions,

$$\int_0^{3\sigma} 2\pi r w \, dr \equiv 1 \ .$$

With $h=3\sigma$, and at unit number density $n\sigma^2\equiv 1$, bulk particles in two dimensions typically interact with 20 to 30 neighbors, providing a sufficiently smooth description of the field variables, as suggested by the numerical results in Fig. 9, discussed later.

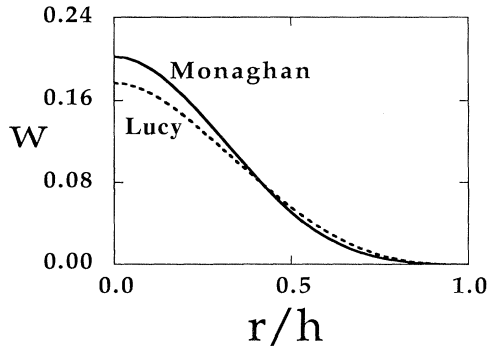

FIG. 1. Lucy's and Monaghan's weight functions $w(r)$. The functions are normalized, with a spatial integral of unity. We have used a range of $h=3\sigma=3(V/N)^{1/2}$.

There are many alternative ways to quantify the smoothness and accuracy of the smooth-particle description. One useful approach, followed in Ref. [5], is based on the observation that a symmetric *lattice* of smooth particles, when used to describe a *fluid,* necessarily corresponds to an extremum of the energy and also typically to a spurious shear modulus. Numerical evaluation of these spurious moduli, as a function of increasing smoothing length, indicates a rapid convergence to zero. Typical shear moduli, for our choice of the smoothing length, are of the order 1% of the bulk modulus.

The main advantage of the smooth-particle method is a simplification of the evaluation of *spatial* derivatives $\{\nabla\rho,\nabla\mathbf{v},\nabla T,\nabla\cdot\mathbf{P},\nabla\cdot\mathbf{Q}\}$, leading to *ordinary,* rather than *partial,* differential equations of motion for the particles. With smooth particles, spatial derivatives can be evaluated in several ways [2], of which two seem to us to be the most useful [5]. To begin, we define the hydrodynamic density, velocity, and energy at a point in terms of sums over nearby particles:

$$\rho(r) \equiv \sum_j m w(\mathbf{r}-\mathbf{r}_j) \ ,$$

$$\rho(\mathbf{r})\mathbf{v}(\mathbf{r}) \equiv \sum_j m\mathbf{v}_j w(\mathbf{r}-\mathbf{r}_j) \ ,$$

$$\rho(\mathbf{r})e(\mathbf{r}) \equiv \sum_j m e_j w(\mathbf{r}-\mathbf{r}_j) \ .$$

The temperature at r, required for heat flux calculations, is evaluated from the density and energy per unit mass by using the thermal equation of state $T(\rho,e)$.

For the *flux-generating* variables, such as the velocity $\mathbf{v}$ which provides the viscous part of the pressure tensor $\mathbf{P}$, and the temperature T which provides the heat flux vector $\mathbf{Q}$, a useful form for the gradients at the smooth-particle locations follows from the gradients of $\rho\mathbf{v}$ and ρT:

$$\nabla(\rho\mathbf{v}) \equiv \rho\nabla\mathbf{v}+\mathbf{v}\nabla\rho \rightarrow$$

$$(\nabla\mathbf{v})_i \equiv \sum_j m[(\mathbf{v}_j-\mathbf{v}_i)/\rho_{ij}]\nabla_i w_{ij} \ ,$$

$$\nabla(\rho T) \equiv \rho\nabla T+T\nabla\rho \rightarrow$$

$$(\nabla T)_i \equiv \sum_j m[(T_j-T_i)/\rho_{ij}]\nabla_i w_{ij} \ .$$

To symmetrize these expressions, the mean density ρ_{ij} can be chosen as either an arithmetic or geometric mean of ρ_i and ρ_j. We have used the geometric mean in all of our work. Knowing the velocity and temperature gradients makes it possible to apply the constitutive relations of Newton and Fourier to associate shear stresses and heat fluxes with each of the smooth particles.

For flows of *conserved* variables, such as the momentum and energy fluxes, an alternative form of space derivative, which provides an exact conservation of momentum and energy in the bulk flow, is preferred:

$$\nabla\cdot(\mathbf{P}/\rho)\equiv(\nabla\cdot\mathbf{P})/\rho-(\mathbf{P}/\rho^2)\cdot\nabla\rho\rightarrow$$
$$(\nabla\cdot\mathbf{P})_i/\rho_i\equiv\sum_j m\,[(\mathbf{P}/\rho^2)_i+(\mathbf{P}/\rho^2)_j]\cdot\nabla_i w_{ij}\ ,$$
$$\nabla\cdot(\mathbf{Q}/\rho)\equiv(\nabla\cdot\mathbf{Q})/\rho-(\mathbf{Q}/\rho^2)\cdot\nabla\rho\rightarrow$$
$$(\nabla\cdot\mathbf{Q})_i/\rho_i\equiv\sum_j m\,[(\mathbf{Q}/\rho^2)_i+(\mathbf{Q}/\rho^2)_j]\cdot\nabla_i w_{ij}\ .$$

With these choices the smooth-particle motion and energy equations become

$$\left\{\ddot{\mathbf{r}}_{\mathrm{SPAM}}\equiv\dot{\mathbf{v}}_i\equiv-\sum_j m\,[(\mathbf{P}/\rho^2)_i+(\mathbf{P}/\rho^2)_j]\cdot\nabla_i w_{ij}+\mathbf{g}\right\},$$

$$\left\{\dot{e}_i\equiv-\sum_j(m/2)[(\mathbf{P}/\rho^2)_i+(\mathbf{P}/\rho^2)_j]:(\mathbf{v}_j-\mathbf{v}_i)\nabla_i w_{ij}\right.$$
$$\left.-\sum_j m\,[(\mathbf{Q}/\rho^2)_i+(\mathbf{Q}/\rho^2)_j]\cdot\nabla_i w_{ij}\right\},$$

where SPAM denotes smooth-particle applied mechanics. As emphasized in Ref. [2], the underlying differential identities, on which the definitions of $\{\nabla\mathbf{v},\nabla T,\nabla\cdot\mathbf{P},\nabla\cdot\mathbf{Q}\}$ are based, are not at all unique, so that other systems of "smooth-particle" equations can be developed. For applications of a different representation of the gradients, using Gaussian weight functions, see Ref. [6].

The smooth-particle approach outlined here is perfectly general, in that *any* constitutive relation can be used. In our own work we have used Newtonian shear viscosity, zero bulk viscosity, and Fourier heat conduction, all with constant transport coefficients, but the method is itself not at all restricted. General dependences of the transport laws on such variables as plastic strain or tensor stress invariants can easily be included. One special case is of particular interest in illuminating some limitations of smooth-particle applied mechanics by relating it to molecular dynamics. This special case [12], in which the pressure varies as ρ^2, is discussed separately in Sec. III. For generality in our hydrodynamic applications, we treat not only the ideal gas constitutive law but also two more realistic dense-fluid equations of state, all with simple linear transport laws.

Because the density, the gradients, and the Eulerian time derivatives at each particle location involve the evaluation of pair sums, the smooth-particle method has to proceed in three separate stages. First, the density at each particle is calculated. Next, the pressure tensors $\{\mathbf{P}\}$, from $\{\nabla\mathbf{v}\}$, and the heat flux vectors $\{\mathbf{Q}\}$, from $\{\nabla T\}$, are worked out. Finally, the pressure and heat flux gradients $\{\nabla\cdot\mathbf{P},\nabla\cdot\mathbf{Q}\}$ are evaluated, allowing $\dot{\mathbf{v}}$ and $\dot{e}$ to be evaluated for each particle. The very smooth nature of the integrands makes the use of the classical fourth-order Runge-Kutta method an efficient approach to the integration of the particle equations. The most time consuming step, finding all those interacting neighbor pairs that lie within a range h, requires implementing a linked-list algorithm [13], with a time proportional to $N\ln N$, where N is the number of particles.

Boundaries provide the crucial link between the fluid system of interest and the surroundings with which it interacts. The boundaries affect the pressure gradients and temperature gradients that govern the particle equations for $\{\dot{\mathbf{v}},\dot{e}\}$. There are two natural ways to confine a system with boundary particles. See Figs. 2 and 3 for examples. First, sufficiently many particles, fixed in space, as well as a leak-proof, perfectly rigid, elastically reflecting wall, can be used. The fixed boundary particles of Fig. 2 provide a high-density container region capable of repelling approaching particles.

At the fixed boundaries both the parallel and the perpendicular velocity components vanish. In implementing the thermal boundaries required in the Rayleigh-Bénard problem, the temperatures of the boundary particles must likewise be fixed. It is nearly as easy, and it is also more "realistic," to use instead a *mirror* boundary condition in which all approaching particles produce reflected images (as shown in Fig. 3). The image particles can be assigned velocities and temperatures independent of all the other particles in their vicinity. For still a different treatment of boundaries, using a *continuous* distribution of external particles, see Ref. [6]. In Sec. IV, we describe the application of both of our discrete-particle boundary approaches to the classic problem of Raleigh-Bénard instability.

III. RELATION OF SMOOTH-PARTICLE APPLIED MECHANICS TO MOLECULAR DYNAMICS

In the special case that the pressure is inviscid and varies as the square of the density $P\propto\rho^2$, the smooth-particle equations of motion

$$\left\{\ddot{\mathbf{r}}_{\mathrm{SPAM}}\equiv\dot{\mathbf{v}}_i\equiv-\sum_j m\,[(\mathbf{P}/\rho^2)_i+(\mathbf{P}/\rho^2)_j]\cdot\nabla_i w_{ij}+\mathbf{g}\right\}$$

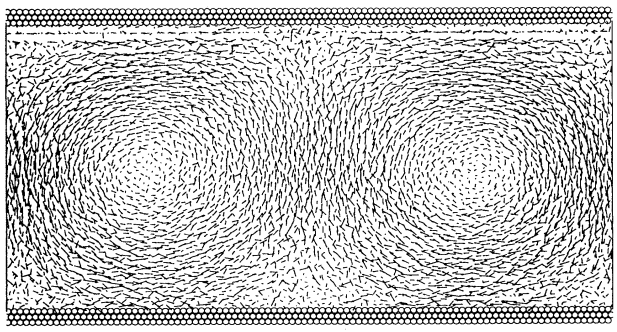

FIG. 2. Rigid boundary rows of fixed particles (with specified temperatures) are used to confine the bulk fluid. The fixed boundary particles are shown as open circles, while the bulk smoothed particles are indicated by arrows with a length proportional to the individual particle velocities. The illustration shows an ideal gas Rayleigh-Bénard flow with $\eta\equiv k/k_B=0.5(m\varepsilon)^{1/2}/\sigma$ at a Rayleigh number of 10 000. There are 5000 bulk particles in a rectangular $50\sigma\times100\sigma$ box.

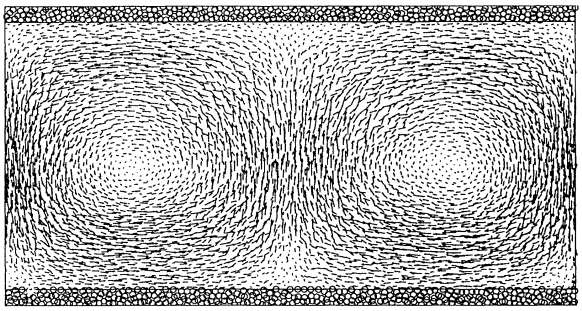

FIG. 3. Reflected image particles follow the motion of corresponding bulk fluid particles, but with specified values of velocity and temperature. The reflected boundary particles are shown as open circles, and the bulk smoothed particles are indicated by arrows with a length proportional to the individual particle velocities. The illustration shows an ideal gas with $\eta \equiv k/k_B = 0.5(m\varepsilon)^{1/2}/\sigma$ at a Rayleigh number of 10 000. There are 5000 bulk particles in a rectangular $50\sigma \times 100\sigma$ box. All particles lying within a distance $3\sigma = 3(V/N)^{1/2}$ of the boundary generate reflected image particles.

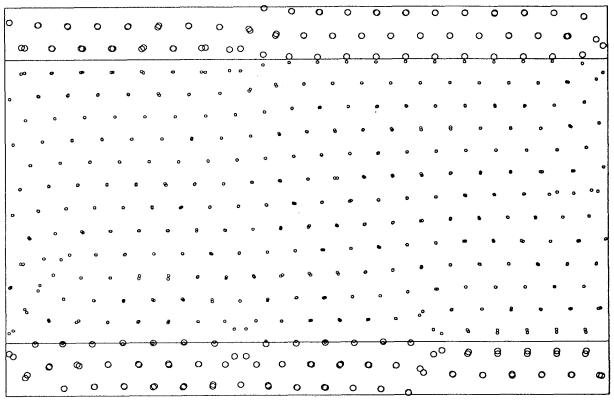

FIG. 4. "Freezing" of the smooth-particle fluid. There are 512 bulk particles in a rectangular $16\sigma \times 32\sigma$ box. A grid-based solution of the Navier-Stokes equations shows that this problem, with a Rayleigh number of 3000 (about twice the critical value) and the dense-fluid equation of state has a convective solution with two rolls. A smooth-particle solution, for the same conditions and equations of state, using Monaghan's weight function with a range $h = 3\sigma$, leads to an unphysical high-pressure freezing out of the smooth-particle motion. Similar results are obtained by using Lucy's weight function.

become identical to the equations of motion of molecular dynamics [5,12,14]

$$\{\ddot{\mathbf{r}}_i \propto -\nabla_i \phi\}_{\rm MD} ,$$

with $w(r)$ playing the role of a pair potential. The resulting smooth-particle trajectories are likewise identical to the classical trajectories of atoms following Newton's equations of motion [12]. Though special, and applying exactly only to the isentropic equation of state for a two-dimensional ideal gas, the quadratic equation of state $P \propto \rho^2$ differs only slightly from that of a three-dimensional isentrope $P \propto \rho^{5/3}$ and is also helpful in understanding *any* fluid flow in which the quotient P/ρ^2 is approximately constant. This isomorphism with molecular dynamics is particularly useful in understanding the peculiar behavior of the smooth-particle equations at high pressure and also provides an interesting version of the reversibility paradox. These two consequences are discussed below.

First, we comment again that smooth-particle applied mechanics necessarily incorporates artificial viscoelastic effects, resulting from the particulate nature of the smooth-particle continuum fields, providing spurious elastic constants and transport coefficients. Even with a "fluid" constitutive equation, sufficiently high pressure can force the underlying smooth particles to freeze, behaving as a (thoroughly artificial) solid. In the very high-pressure case $P \to \infty$, no pair of smooth particles can have a separation lying between 0 and h. This causes a peculiar limiting lattice structure with many particles per site. Though these spurious effects vanish as the range of the weighting function increases [5], in certain circumstances—an example, with two particles per site, appears in Fig. 4—they give rise to qualitative, as opposed to quantitative, errors in simulations. Accurate applications of the smooth-particle approach require that these spurious effects be negligibly small. A detailed analysis of this artificial freezing out of convective motion appears in Sec. IV.

Second, in addition to emphasizing the practical need for vigilance in simulating fluid flow with smoothed particles, the isomorphism of smooth-particle trajectories to atomistic ones is also relevant to an academic understanding of the irreversibility paradox Boltzmann studied over a century ago. Boltzmann devoted much of his lifetime to understanding and explaining the fact that microscopic particles, obeying Newton's time-reversible equations of motion, can give rise to macroscopic hydrodynamic irreversibility, as described by the second law of thermodynamics. In our special case, the smooth-particle analysis of a two-dimensional ideal gas, the macroscopic equations being represented are the time-reversible Euler equations for an inviscid nonconducting fluid, but the model used to describe them is expected to be that of a fluid composed of particles interacting with the potential function $w(r)$, and hence having an atomistic viscosity and heat conductivity. Thus Boltzmann's paradox (microscopic reversibility $\to$ macroscopic irreversibility) is *reversed* for the smooth-particle representation [macroscopic time-reversible equations $\to$ (irreversible) microscopic molecular dynamics]. The exact reversibility of the smooth-particle equations, and their relation to molecular dynamics for an Euler fluid, has recently been analyzed in detail [12].

IV. RAYLEIGH-BÉNARD SIMULATION WITH SPAM

For fluids that expand when heated, the effect of gravitational forces on the resulting density gradient can lead to convection currents [4,5]. Then heat is transported more efficiently, by a combination of conduction and convection. This situation is shown in Figs. 2 and 3, where the gravitational acceleration is downward while the

motionless top and bottom boundaries are held fixed at cold and hot temperatures, respectively. We have simulated such prototypical Rayleigh-Bénard problems by using both Lucy's and Monaghan's weight functions with three different equations of state, given in Eqs. (1–3) below. The simplest of the three state equations is the ideal gas law, appropriate to a dilute gas,

$$P=\rho e, \quad \beta e = e/k_B T = 1 , \tag{1}$$

where k_B is Boltzmann's constant *per unit mass*. We have also used van der Waals' fluid equation of state (2) and a typical dense-fluid equation of state (3) as determined by a set of molecular-dynamics simulations [4].

Van der Waals' equation applies to both gases and liquids. The equation augments the ideal-gas equation of state to include both the effects of attractive forces (through parameter a) and excluded volume effects (through parameter b). In the single-phase region of the phase diagram,

$$\beta P = [\rho/(1-\rho b)] - \beta a \rho^2, \quad \beta e = 1.0 - \beta \rho a ,$$
$$a \equiv \varepsilon\sigma^2/2m^2, \quad b = \sigma^2/2m . \tag{2}$$

We choose these values for the two material properties, a and b, so that the unit reduced number density $n\sigma^2 = N\sigma^2/V = \rho\sigma^2/m = 1$ somewhat exceeds the critical reduced number density (2/3) and that our reduced temperature range $0.5 < mk_B T/\varepsilon < 1.5$ lies well above the critical reduced temperature $mk_B T_c/\varepsilon = (8/27)$.

In addition to the ideal gas and van der Waals models, we have also used a more complex equation of state [4] from molecular dynamics—a quadratic expansion of the pressure and energy about a reference state at unit reduced density and temperature:

$$PV/N\varepsilon = 5 + 8\delta n + 2.5\delta u + 9(\delta n)^2 + 2\delta n \delta u ,$$
$$mk_B T/\varepsilon = 1 - \delta n + 0.7\delta u - 0.8(\delta n)^2 - 0.5\delta n \delta u ,$$
$$u \equiv me/\varepsilon \equiv E/N\varepsilon = 1.443 + 1.5\delta n + 1.5\delta\tau + 2.4(\delta n)^2 + 1.2\delta n \delta\tau , \tag{3}$$
$$\delta n \equiv n\sigma^2 - 1.0 ,$$
$$\delta u \equiv (E/N\varepsilon) - 1.443 ,$$
$$\delta\tau \equiv (mk_B T/\varepsilon) - 1.000 .$$

At the reference state the reduced energy and pressure are given by $u = E/N\varepsilon = 1.443$ and $P\sigma^2/\varepsilon = 5$. Notice that we use u to indicate a reduced energy. The thermal equation of state, linking energy to temperature, is required for heat flux calculations.

It should be noted that this quadratic dense-fluid equation of state (3) is not quite "thermodynamically consistent." For instance, the Maxwell relation based on differentiating Helmholtz's free energy A with respect to temperature and volume

$$\partial^2(\beta A)/\partial\beta\partial V = (\partial E/\partial V)_T = \partial^2(\beta A)/\partial V \partial\beta = -\partial[(\beta P)/\partial\beta]_V ,$$
$$\beta \equiv 1/mk_B T$$

is not exactly satisfied. This means that thermodynamic cycles can be constructed in such a way as to violate conservation of energy. To illustrate, consider just linear variations around the reference state. $(\partial E/\partial V)$, evaluated from the energy equation, is $-1.5\varepsilon/\sigma^2$, whereas $\partial(\beta P)/d\beta = P + \partial P/\partial \ln\beta$, evaluated by combining the mechanical equation of state and the energy equation, is $1.25\varepsilon/\sigma^2$. This lack of consistency causes no apparent trouble in smooth-particle simulations. On the other hand, we believe that it is the underlying cause of a slow divergence, at very long times, of some of our attempts to find corresponding Navier-Stokes "solutions."

Our dense-fluid equation of state (3) was especially useful in revealing a fundamental shortcoming of the smooth-particle method in treating dense fluids at very high pressures. Our early attempts to compare Navier-Stokes and smooth-particle solutions for the molecular-dynamics-based equation of state led repeatedly to "frozen" states, with the smooth particles crystallizing into static hexagonal-symmetry structures with either one (Lucy) or two (Monaghan) particles per site. See Fig. 4, for example. With exactly the same imposed boundary conditions, the Navier-Stokes equations easily generated reproducible convecting flows.

This unphysical high-pressure freezing can be traced to the form of the smooth-particle equation of motion, as discussed in Sec. III. At sufficiently low pressures a typical smooth-particle kinetic energy exceeds the maximum value of the effective potential energy from which the smooth-particle accelerations are determined:

$$mv^2 > \phi(0) = 2P(V/N)^2 w(0) .$$

At sufficiently high pressure, on the other hand, $P(V/N)$ approximates mc^2, where c is the speed of sound, so that ordinary hydrodynamic flows, with compressibility but with velocities much smaller than the speed of sound, cannot overcome the potential barrier to smooth-particle motion.

A more precise criterion for the applicability of the smooth-particle technique for fluids can be based on an analog of Lindemann's melting criterion. In two or three space dimensions, melting occurs when the fluctuation in the nearest-neighbor separation is of the order of 10%. For the corresponding potential energy to be available from the flow, the pressure cannot be too large:

$$mv^2 > 2Pn^{-2}[w(0.9\sigma) - w(\sigma)] .$$

For our Lucy weight function, the combination in square brackets is about $0.01n$. The dense-fluid equation of state (2), which was fitted to a set of equilibrium molecular-dynamics simulations, has $2Pn^{-1} \approx mc^2$, where c is the sound speed. Under supercritical and moderately dense conditions, the van der Waals equation of state (2) has a considerably lower pressure relative to the speed of sound. Thus, though the smooth-particle approach provides a good description of the van der Waals flow as well as ideal-gas flows based on (1), it can fail to describe convection—as shown in Fig. 4—for the alternative equation of state given in (3). The difference lies in the smooth-particle treatment of the pressure gradient. In

conventional continuum mechanics, a constant pressure addition does not affect the accelerations at all because they depend upon the *gradient* $\nabla\cdot\mathbf{P}$. In smooth-particle mechanics such an addition *does* affect the accelerations, through the combination $(\mathbf{P}/\rho^2)\cdot\nabla w$.

In our smooth-particle work we have used not only two different types of boundary conditions, fixed particles and moving reflected image particles, but also two different system shapes, with aspect ratios of 1 and 2, in order to make contact with earlier calculations [7–11]. A system with periodic lateral boundaries and an aspect ratio of 2 corresponds closely to Chandrasekhar's classical analysis [7], which predicts—for sticking boundaries—that stable convection begins to occur as the Rayleigh number exceeds 1708. A square system, with specified temperature on the boundaries, corresponds to the simulation of Goldhirsch, Pelz, and Orszag, using a spectral method [9]. These workers did not estimate the precise critical Rayleigh number for this system. In both cases we control the boundary values of temperature and velocity by specifying these for all image particles.

Both Chandrasekhar and Goldhirsch-Pelz-Orszag consider the nearly incompressible Boussinesq approximation. This leads to small but definite deviations of our fully compressible results from theirs, as is discussed quantitatively in Sec. V. Though we first believed that the small deviations from Chandrasekhar's analysis were due to our relatively large temperature gradient (with $\Delta T \approx \langle T \rangle$), additional calculations with much smaller temperature differences ΔT produced only small changes, so we believe that the Boussinesq approximation is responsible for the disagreements. The usual theoretical perturbation analyses typically assume either an isochoric or an isobaric thermal diffusivity. In fact, for a compressible fluid, any hydrodynamic process is neither isochoric nor isobaric, so that an intermediate heat capacity is appropriate. A short discussion of the limitations of the Boussinesq approximation, with references, appears in Ref. [15].

In addition to the equilibrium equation of state, irreversible momentum and energy transport must be described. For simplicity, we have in every case chosen constant, and equal, reduced transport coefficients, corresponding to a Prandtl number of unity. We have explored the two simplest choices. First,

$$\eta \equiv k/k_B \propto (m\varepsilon)^{1/2}/\sigma \ ,$$

where η is the shear viscosity, k is the thermal conductivity, and k_B is Boltzmann's constant per unit mass. Second,

$$\nu \equiv \eta/\rho \equiv \kappa \equiv k/(\rho C_V) \propto (\varepsilon/m)^{1/2}\sigma \ ,$$

where ν is the kinematic viscosity and κ is the thermal diffusivity $\kappa \equiv k/(\rho C_V)$. C_V is the isochoric specific heat. The transport coefficients η and k are defined by Newton's and Fourier's laws:

$$P_{xy} = -\eta[(\partial v_x/\partial y)+(\partial v_y/\partial x)], \quad Q_y = -k\,\partial T/\partial y \ .$$

Though the two choices above are equivalent for the reference state, they in fact lead to slightly different critical Rayleigh numbers, close to, and bracketing, Chandrasekhar's analytic result based on the Boussinesq approximation.

In the continuum simulations we have assigned the densities and fluxes of image particles to match those of the corresponding bulk particles. Thus the density and fluxes are continuous at all system boundaries. To satisfy the condition of static equilibrium at an exactly constant density, we have further chosen the magnitude of the gravitational acceleration to satisfy the static force balance equation

$$(\partial P/\partial T)_\rho dT - \rho g\, dy = 0 \ .$$

Thus, for the ideal gas equation of state, g is chosen equal to $k_B\Delta T/L$, where mk_B is Boltzmann's constant, L is the system height, and ΔT is the temperature difference $T_{\rm hot} - T_{\rm cold}$. For the dense-fluid and van der Waals equations of state, we have used the same constant-density condition, evaluating the thermodynamic derivative $(\partial P/\partial T)_\rho$. All of our simulations have been carried out with the overall reduced density equal to unity; most have a mean reduced temperature $mk_B\langle T\rangle/\varepsilon = (mk_B/\varepsilon)[T_{\rm hot}+T_{\rm cold}]/2$ of unity as well.

V. CONTINUUM FLOW SOLUTIONS WITH A REGULAR GRID

We obtained grid-based continuum solutions in order to test the accuracy of our smooth-particle results, though one aspect of these solutions, as discussed below and illustrated in Figs. 5 and 6, has some independent interest of its own. Only a brief description of our method for solving the Navier-Stokes equations is warranted because the approach we developed turned out not to be new [11]. We spanned the system with a grid of square cells, evaluating $\{\mathbf{v}, e, \partial\mathbf{v}/\partial t, \partial e/\partial t\}$ at the grid points and $\{\rho, \mathbf{P}, \mathbf{Q}, \partial\rho/\partial t\}$ at the cell centers. The centered-difference equations for the time development of $\{\rho, \mathbf{v}, e\}$ at these fixed locations were integrated with the same fourth-order Runge-Kutta integrator that we used in the smooth-particle work. The required values of density from cell centers just outside the system were set equal to the nominally constant reference-state value of unity. With this scheme we found no trouble in obtaining fully converged results for systems of several thousand cells.

Two aspects of the continuum results were especially interesting. First, we found that there is a considerable range of Rayleigh number values (from roughly the critical value, at which flow begins, to four times that value, as shown in Figs. 5 and 6) for which the kinetic energy of the convective rolls varies almost exactly linearly when plotted as a function of $\mathrm{Ra}^{-1/2}$. Furthermore, the slopes and intercepts of these lines also varied almost exactly linearly with L^{-2}. These two simple linear dependences made it possible to extrapolate accurately (five significant figures can easily be obtained) to a fully converged critical Rayleigh number using just a few calculations, with either $N\times N$ or $N\times 2N$ square zones and with N values of 30, 40, 50, ... Such highly accurate extrapolated re-

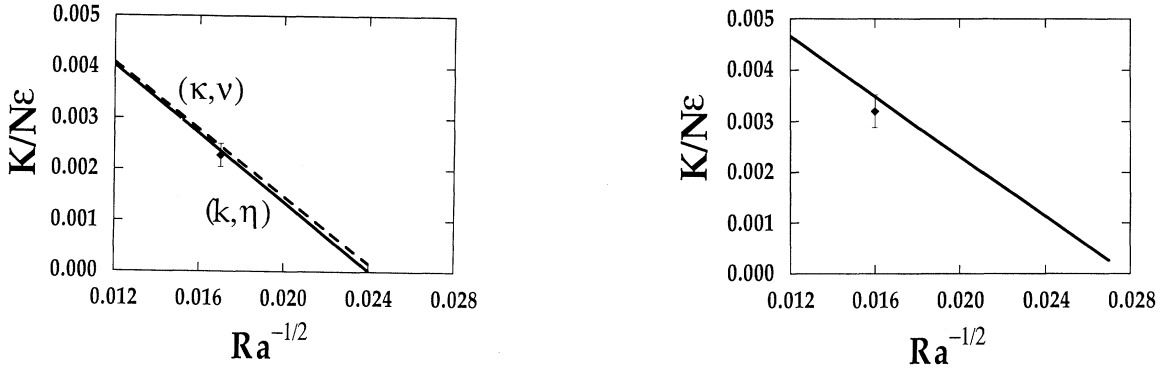

FIG. 5. Fully converged ($L \to \infty$) variation of reduced kinetic energy $K/N\varepsilon$ with Rayleigh number Ra with periodic lateral boundaries, fixed upper and lower boundaries, an aspect ratio of 2, and $\eta \equiv k/k_B \propto (m\varepsilon)^{1/2}/\sigma$. Both ideal gas (left) and van der Waals (right) results are shown. In the ideal-gas case additional results using $\nu \equiv \eta/\rho \equiv \kappa \equiv k/(\rho C_V) \propto (\varepsilon/m)^{1/2}\sigma$ are included for comparison. The Lucy-weighted smooth particle points shown, for comparison to the Navier-Stokes solutions, are the results of simulations using 5000 particles.

sults are shown in Figs. 5 and 6 for the two kinds of boundary conditions. These numerical results make it possible to assess the accuracy of the smooth-particle solutions discussed in Sec. VI.

VI. SMOOTH-PARTICLE APPLIED MECHANICS FLOW SOLUTIONS

Our smooth-particle calculations were typically carried out with from 500 to 5000 particles, though even a million particles could be used on a modern parallel computer. Five hundred particles can easily generate convincing and realistic convection currents. See Fig. 7 for a 512-particle flow using van der Waals' equation of state.

Not only the final states of these simulations but also the approach to these convecting states are described semiquantitatively, with errors of the order of a few percent. In Fig. 8 we compare the approach to the steady state for an ideal gas using the smooth-particle method to that found by solving the Navier-Stokes equations, as described in Sec. V. In both cases we use the same simple initial velocities

$$v_x \propto \sin(\pi x/L)\sin(2\pi y/L), \quad -L < x < +L ,$$

$$v_y \propto \cos(\pi x/L)\cos(\pi y/L), \quad -L/2 < y < +L/2$$

with an internal energy distribution corresponding to a uniform temperature gradient.

Errors of less than about 1% are disguised by the fluctuations inherent in the smooth-particle method. These fluctuations are the analog of kinetic temperature in molecular dynamics, a measure of the mean-squared deviation of individual particle velocities from the average velocity in their neighborhood, $\langle v^2 \rangle - \langle v \rangle^2$. Because the kinetic energy of the continuum flows was found to vary nearly linearly with $\mathrm{Ra}^{-1/2}$, we have chosen the kinetic

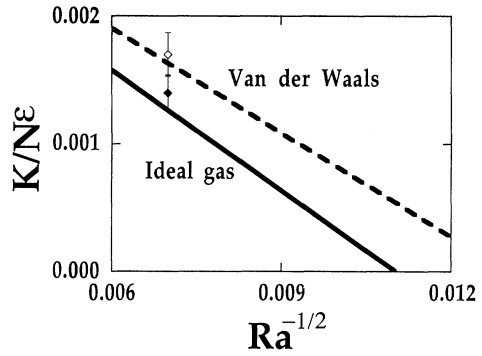

FIG. 6. A fully converged ($L \to \infty$) variation of reduced steady-state kinetic energy $K/N\varepsilon$ with the Rayleigh number Ra in square systems with four reflecting boundaries. The temperature along the lateral boundaries is a linear interpolation between the temperatures of the two horizontal boundaries. The points shown are the results of corresponding Lucy-weighted smooth-particle simulations using 1600 particles.

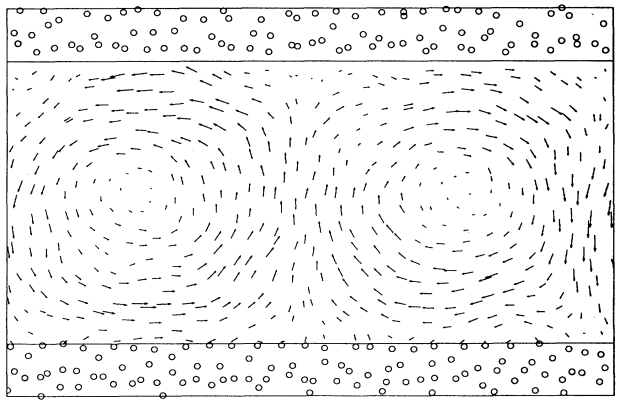

FIG. 7. Rayleigh-Bénard simulation of a van der Waals fluid using Lucy's weight function. There are 512 bulk particles in a rectangular $16\sigma \times 32\sigma$ box. The mean reduced number density $n\sigma^2 = 1$ is half the maximum, and the mean temperature is 27/8 times the critical temperature.

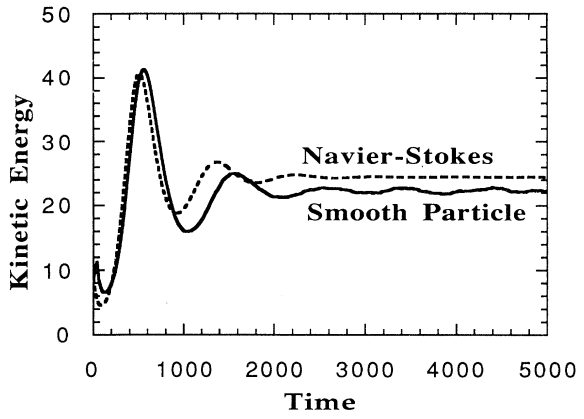

FIG. 8. Approach of the kinetic energy to the steady two-roll state for the continuum and Lucy-weighted smooth-particle methods, applied to an ideal gas [Rayleigh numbers 10 000 and $\eta \equiv k/k_B = 0.5(m\varepsilon)^{1/2}/\sigma$]. The initial condition has a uniform temperature gradient and two simple rolls, with the functional form given in Sec. VI corresponding to a total kinetic energy about one half the final value.

energy of the smooth-particle flows $(\rho/2)\langle v \rangle^2$ for a quantitative comparison. We compared the Navier-Stokes and smooth-particle kinetic energies per unit mass for Rayleigh numbers 5000 and 10 000. A comparison at a still lower Rayleigh number of 2500 was abandoned. In this last case the smooth-particle simulation exhibited relatively large fluctuations, while fluctuations are ignored in the hydrodynamic solution. From the Navier-Stokes calculations, the corresponding infinitely fine-mesh limits are 0.003 40 and 0.004 81 for Rayleigh numbers 5000 and 10 000. From the smooth-particle results, using the ideal-gas equation of state, these same specific energies are 0.003 0 and 0.004 6. Thus the energy errors are no worse than 10%, so that velocity errors are of the order of 5%. Smooth-particle kinetic-energy data are also shown in Figs. 5 and 6, again with velocity fields correct to about 5%. Comparisons of the density and temperature contours appear in Fig. 9. We view the good agreement of the smooth-particle and the Navier-Stokes results as completely satisfactory, provided the pressure is low enough to allow for smooth-particle fluid flow.

Figure 10 displays an interesting feature associated with Monaghan's weight function with $h/\sigma = 3$ and at unit reduced density. The smooth particles have a tendency to move in closely associated pairs. This feature is common to both the flows (an ideal gas and a dense fluid) shown in the figure. Under these same conditions Lucy's weight function shows no such pairing phenomenon. In the ideal-gas case the two rolls shown in the figure give way to a single roll at lower values of the Rayleigh number.

At higher values of the Rayleigh number the "robust" smooth-particle technique continues to provide solutions when our centered-difference regular-grid continuum solutions begin to fluctuate. In this regime more sophisticated grid-based techniques would be required for a quantitative comparison with the SPAM simulations. It is the robust, highly stable aspect of smooth-particle applied mechanics, for extreme conditions and at high speeds, that accounts for its popularity in studying a variety of strongly nonequilibrium fluid and solid flows [3].

We ourselves have used the method to study the in-

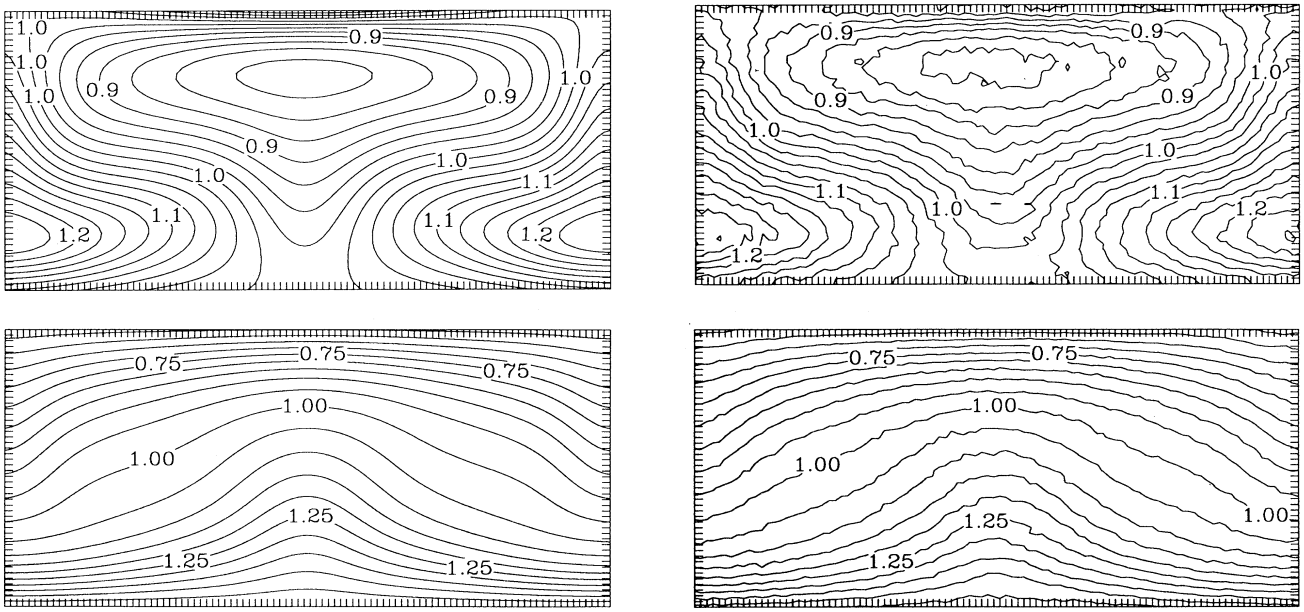

FIG. 9. Density (upper) and temperature (lower) distributions for the continuum (left) and smooth-particle (right) methods using the ideal-gas equation of state with $\eta \equiv k/k_B = 0.5(m\varepsilon)^{1/2}/\sigma$. There are 5000 bulk particles in a rectangular $50 \times 100\sigma$ box. The Rayleigh number is 10 000 and the aspect ratio is 2. The total initial kinetic energy of the 5000 particles was about 9ε. The distributions correspond to a time of $5000(m\sigma^2/\varepsilon)^{1/2}$.

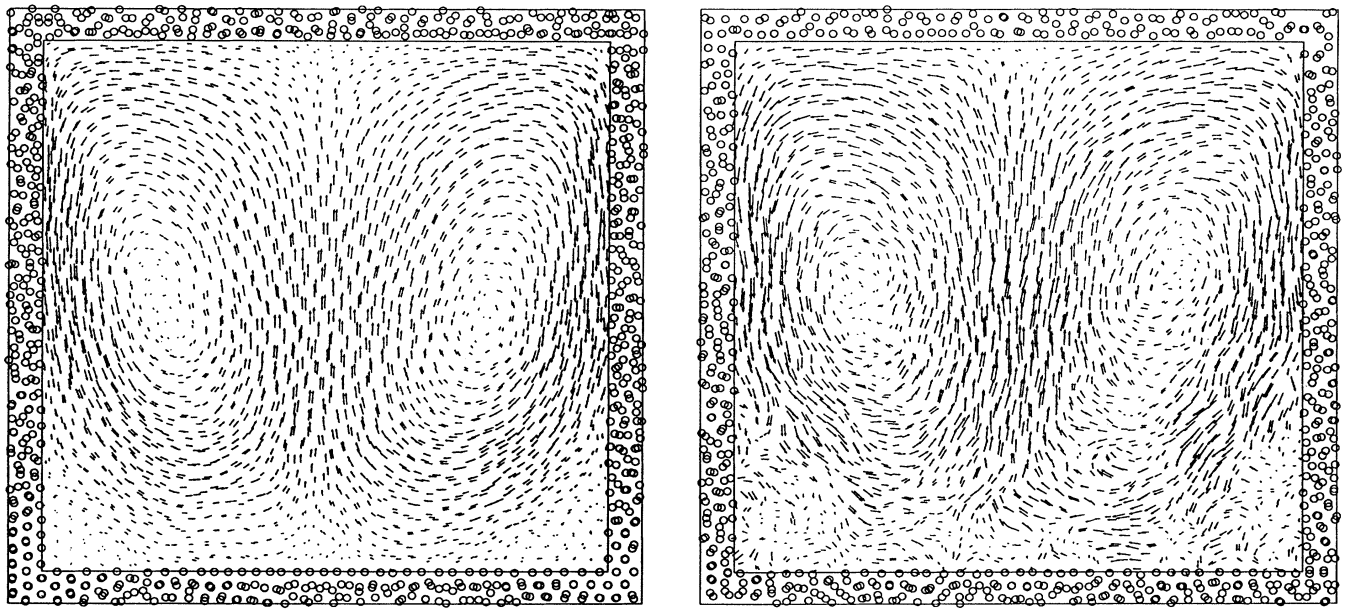

FIG. 10. Two Rayleigh-Bénard simulations with temperatures of $10.0\varepsilon/mk_B$ and $0.5\varepsilon/mk_B$, using Monaghan's weight function. There are 2500 bulk particles in a rectangular $50\sigma \times 50\sigma$ box. The left-hand simulation uses the ideal gas equation of state, and the right hand simulation uses the empirical dense-fluid equation of state described in the text. The transport coefficients are $\eta \equiv k/k_B = 0.8(m\varepsilon)^{1/2}/\sigma$ in the ideal-gas case and $0.4(m\varepsilon)^{1/2}/\sigma$ in the dense-fluid case. The gravitational field strength was chosen to give a Rayleigh number of 350 000 in both cases. In the ideal gas the two rolls merged into one for small Rayleigh numbers near the critical value. Temperature varies linearly with distance along the vertical sides of the box.

teraction of strong shock waves with material interfaces, the "Richtmyer-Meshkov" instability, and found good agreement with theoretical estimates of the instability growth rate [5]. A sample simulation result, for the growth of a sinusoidal interface perturbation under shock wave conditions, is shown in Fig. 11. The corresponding perturbation growth rate agreed with linear stability theory to within 2% in this case [5].

VII. CONCLUSIONS

Smooth-particle applied mechanics provides a robust and simple approach to reasonably accurate solutions of many continuum problems, including Rayleigh-Bénard instability. It completely avoids grid-tangling and mesh instabilities. In some cases, smooth-particle solutions require many fewer degrees of freedom than do equally ac-

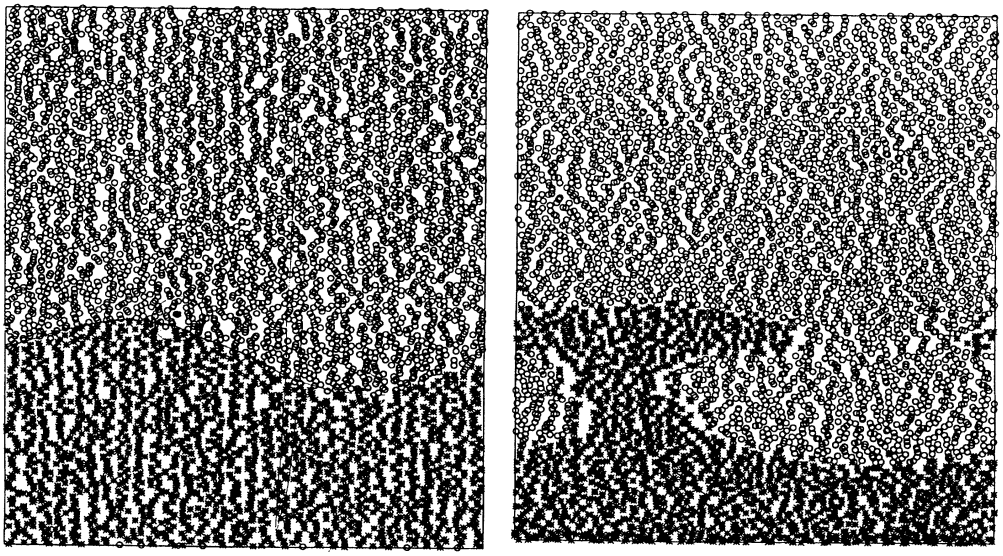

FIG. 11. Time development of a sinusoidal shock front perturbation using a smooth-particle description for two ideal gases initially differing by a factor of 4 in density. The width of the system is 30σ. The height is 100σ. The early growth rate of the interface perturbation is approximately linear in the time and lies within 2% of the theoretical calculation, as is described in Ref. [5].

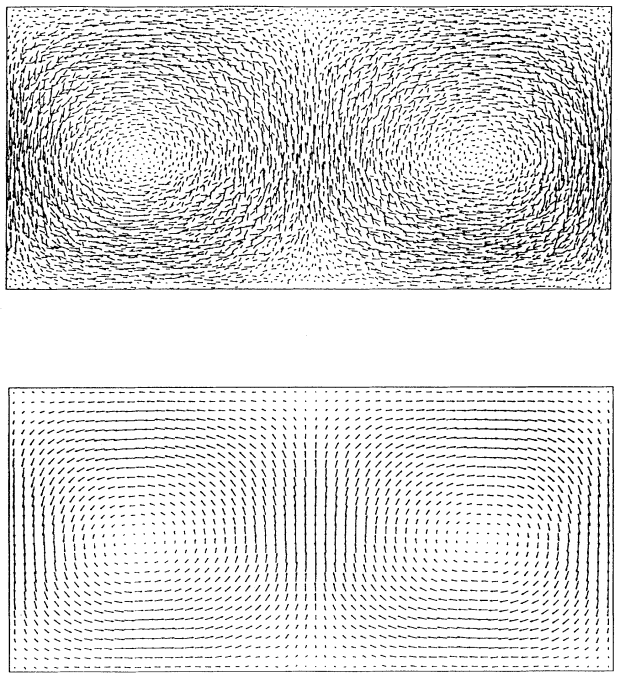

FIG. 12. Two equivalent views of an ideal gas simulation at a Rayleigh number of 10 000 and with $\eta \equiv k/k_B = 0.5(m\varepsilon)^{1/2}\sigma$. There are 5000 bulk particles in a rectangular $50\sigma \times 100\sigma$ box. In the lower view the velocities have been evaluated on an 1800-point square grid, still covering the same $50\sigma \times 100\sigma$ area, using Lucy's weight function with a range of $3\sigma \equiv 3(V/N)^{1/2}$. The distributions correspond to a time of $5000(m\sigma^2/\varepsilon)^{1/2}$.

curate finite-difference or finite-element solutions. Considerably fewer smooth particles are required than atoms in corresponding molecular-dynamics simulations of Rayleigh-Bénard convection, for instance. Nevertheless, the smooth-particle trajectories are essentially Newtonian trajectories, for particles with mass m, subject to an effective potential function $2Pn^{-2}w(r)$. Accordingly, high-pressure subsonic problems, with $v^2 \ll c^2$, cannot be reliably solved by using this method.

The smooth-particle method promises to be of special interest whenever it is desirable to include fluctuations or to evaluate accurate flow quantities on a regular grid. This latter feature is desirable for the calculation of fast Fourier transforms of field quantities and for automatic rezoning. Figure 12 illustrates two velocity-arrow views of the same flow field: first, the individual smooth-particle velocities; second, the averaged flow velocities computed at the vertices of a square grid. Because the smooth-particle results we find lie within a few percent of fully converged solutions of the compressible continuum equations, it is economically desirable to develop this method further.

Although we have not carried out detailed studies it is clear that the convergence of the smooth-particle approximation to a compressible continuum fluid or solid also guarantees convergence of the long-wavelength density fluctuations to the corresponding Debye spectrum.

ACKNOWLEDGMENTS

The work described here was supported by (i) the Lawrence Livermore National Laboratory, under the auspices of the United States Department of Energy, Contract No. W-7405-Eng-48; (ii) the Agency for Defense Development, Republic of Korea; and (iii) an Interuniversity Transfer Agreement for the support of Oyeon Kum. We thank Bill Ashurst, Larry Cloutman, Matt Gibbons, Brad Holian, Carol Hoover, Doug Miller, and Alan Spero for useful and constructive comments on many aspects of this work and Jeff Swegle for kindly providing us with copies of his unpublished Sandia Corporation reports.

[1] L. B. Lucy, Astron. J. **82**, 1013 (1977).
[2] J. J. Monaghan, Ann. Rev. Astron. Astrophys. **30**, 543 (1992).
[3] *Advances in the Free-Lagrange Method,* Lecture Notes in Physics No. 395, edited by H. E. Trease, M. J. Fritts, and W. P. Crowley (Springer-Verlag, Berlin, 1991).
[4] W. G. Hoover, T. G. Pierce, C. G. Hoover, J. O. Shugart, G. M. Stein, and A. L. Edwards, Comput. Math. Applic. **28**, 155 (1994).
[5] O. Kum, Ph.D. thesis, University of California at Davis/Livermore, 1995.
[6] H. Takeda, S. M. Miyama, and M. Sekiya, Prog. Theor. Phys. **92**, 939 (1994).
[7] S. Chandrasekhar, *Hydrodynamic and Hydromagnetic Stability* (Oxford, London, 1961).
[8] D. C. Rapaport, Phys. Rev. Lett. **60**, 2480 (1988).
[9] I. Goldhirsch, R. B. Pelz, and S. A. Orszag, J. Fluid Mech. **199**, 1 (1989).
[10] T. Watanabe, H. Kaburaki, and M. Yokokawa, Phys. Rev. E **49**, 4060 (1994).
[11] A. Puhl, M. M. Mansour, and M. Mareschal, Phys. Rev. A **40**, 1999 (1989).
[12] O. Kum and W. G. Hoover, J. Stat. Phys. **76**, 1075 (1994).
[13] R. W. Hockney and J. W. Eastwood, *Computer Simulation Using Particles* (McGraw-Hill, New York, 1981).
[14] H. A. Posch, W. G. Hoover, and O. Kum, Phys. Rev. E **52**, 1711 (1995).
[15] S. Paolucci and D. R. Chenoweth, Phys. Fluids **30**, 1561 (1987).